Technical Report Documentation Page

1. Report No.	2. Government Accession No.	3. Recipient's Catalog No.
FHWA/TX-95-1305-2		

4. Title and Subtitle	5. Report Date
FACTORS AFFECTING THE DESIGN THICKNESS OF BRIDGE SLABS: RESULTS OF STATIC AND FATIGUE TEST	December 1994
	6. Performing Orgonization Code
7. Author(s)	8. Performing Organization Report No.
Ned H. Burns, Richard E. Klingner, and Jubum Kim	Research Report 1305-2
9. Performing Organization Name and Address	10. Work Unit No. (TRAIS)
Center for Transportation Research The University of Texas at Austin 3208 Red River, Suite 200 Austin, Texas 78705-2650	11. Contract or Grant No. Research Study 0-1305
	13. Type of Report and Period Covered
12. Sponsoring Agency Name and Address Texas Department of Transportation Research and Technology Transfer Office P. O. Box 5051 Austin, Texas 78763-5051	Interim
	14. Sponsoring Agency Code

15. Supplementary Notes

Study conducted in cooperation with the U.S. Department of Transportation, Federal Highway Administration. Research study title: "Factors Affecting Design Thickness of Bridge Slabs"

16. Abstract

The punching shear behavior of concrete bridge decks under static, pulsating fatigue, and rolling fatigue loads was studied using analytical and experimental models. In this report, study results are presented for static and pulsating fatigue loads on cast-in-place and precast, prestressed panel bridge decks. Complete study conclusions will be presented and discussed in the final project report.

17. Key Words	18. Distribution Statement
Punching shear behavior, static loads, pulsating fatigue loads, rolling fatigue loads, analytical models, experimental models, cast-in-place bridge decks, precast prestressed panel bridge decks	No restrictions. This document is available to the public through the National Technical Information Service, Springfield, Virginia 22161.

19. Security Classif. (of this report)	20. Security Classif. (of this page)	21. No. of Pages	22. Price
Unclassified	Unclassified	52	

FACTORS AFFECTING THE DESIGN THICKNESS OF BRIDGE SLABS: RESULTS OF STATIC AND FATIGUE TEST

by

Ned H. Burns, Richard E. Klingner and Jubum Kim

Research Report Number 1305-2

Research Project 0-1305
Factors Affecting Design Thickness of Bridge Slabs

conducted for the

TEXAS DEPARTMENT OF TRANSPORTATION

in cooperation with the

U.S. DEPARTMENT OF TRANSPORTATION
FEDERAL HIGHWAY ADMINISTRATION

by the

CENTER FOR TRANSPORTATION RESEARCH
Bureau of Engineering Research
THE UNIVERSITY OF TEXAS AT AUSTIN

December 1994

IMPLEMENTATION

This report concerns a testing program to evaluate the factors affecting the design thickness of bridge slabs, with emphasis on the behavior of bridge decks in punching shear fatigue. Results of this report are not intended for implementation at this time. Implementation of the complete study results will be discussed in the final project report.

Prepared in cooperation with the Texas Department of Transportation and the U.S. Department of Transportation, Federal Highway Administration.

Ned H. Burns, Texas P.E. #20801
Richard E. Klingner, P.E. #42483

Research Supervisors

TABLE OF CONTENTS

LIST OF FIGURES

LIST OF TABLES

SUMMARY

The punching shear behavior of concrete bridge decks under static, pulsating fatigue, and rolling fatigue loads was studied using analytical and experimental models. In this report, study results are presented for static and pulsating fatigue loads on cast-in-place and precast, prestressed panel bridge decks. Complete study conclusions will be presented and discussed in the final project report.

CHAPTER ONE

INTRODUCTION

1.1 GENERAL

Over the past decades, considerable research has been conducted on the load carrying capacity of the reinforced concrete bridge decks. The flexural capacity of bridge decks may be increased by in-plane compressive forces, created when the deck has undergone flexural cracking. This phenomenon, known as "arching action," has led to new design approaches for bridge decks, requiring less flexural reinforcement than previous design approaches [2,3,4,5,6,7,8,14]. Since flexural capacity is increased by this arching action, the capacity of bridge decks is controlled by punching shear [1-15]. However, research pertaining to punching shear in bridge decks, especially in fatigue, was limited.

Thus, the objective of this project was to investigate the effects of fatigue deterioration on the punching shear resistance of bridge decks, under the sponsorship of the Texas Department of Transportation (TxDOT).

1.2 OBJECTIVES AND SCOPE

The general purpose of Texas Department of Transportation Project 3-15D-92-1305 is to develop guidelines that will specify the required thickness of bridge decks as a function of various characteristics, such as loading level, wheel spacing, and fatigue history. To determine these guidelines, the fatigue behavior of concrete slabs must be carefully studied. This consists of testing slabs in different types of fatigue, and plotting "S-N curves," which display maximum stress range of the slabs versus the number of fatigue cycles to failure. Investigation is conducted on commonly used bridge deck configurations: cast-in-place reinforced concrete bridge decks; and precast, prestressed panel decks.

The specific objectives for Project 1305 are as follows:

1) To review past research pertaining to the wheel load, axle width, and axle spacing characteristics of standard and nonstandard loads.

2) To use structural analysis computer programs and engineering models to estimate the stress range experienced by a full-scale cracked bridge deck subjected to a conventional truck loading, and to predict the maximum principal tensile stress in the cracked deck.

3) To design and construct a test setup that will allow for the static and dynamic testing of full-scale bridge decks, including both rolling and pulsating (constant location) loads.

4) To develop S-N curves for both cast-in-place reinforced concrete decks and precast, prestressed panel decks, and to use these curves to determine the effects of rolling versus fixed load applications, and of arching action.

5) To recommend guidelines for specifying the required thickness of bridge deck slabs as a function of traffic characteristics.

The purpose of this report is to describe the research development on the effects of fatigue on the punching shear capacity of a bridge deck, following the work noted in previous report [1]. This includes a refined finite element analysis, the design and implementation of testing apparatus and testing frame, and the presentation and discussion of test results for static loads, pulsating fatigue loads, and rolling fatigue loads on cast-in-place reinforced concrete bridge decks.

The objectives of the work described in this report were as follows:

1) To develop a refined finite element model for the test specimen which can represent and predict the behavior of the bridge decks.

2) To design and implement a testing apparatus, test setup and test specimens.

3) To present experimental test results for cast-in-place bridge decks under static and pulsating fatigue loads.

4) To present the experimental results from rolling fatigue tests and to correlate the slab behavior with that from pulsating fatigue tests.

CHAPTER TWO

BACKGROUND

2.1 INTRODUCTION

In this chapter, an overview on arching action in concrete bridge decks, fatigue characteristics on concrete structure, and a review of past research of project 1305 are presented. Much of the material reviewed in this chapter is adapted from a prior report submitted to TxDOT for this project [1].

2.2 ARCHING ACTION

When an uncracked bridge deck undergoes traffic loading, it acts primarily as a one-way system, resisting load by transverse flexure. In-plane action remains insignificant in bridge decks before flexural cracking. However, once the deck cracks near the point of loading and above the supports, it acts as a flat dome.

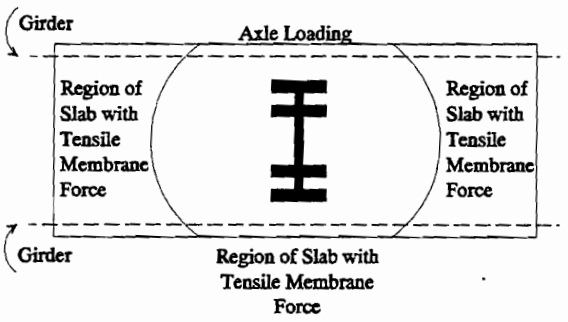

Figure 2- 1 Zone of compression balanced by surrounding zone of tension, arching action

This "dome" is defined by a compression zone near the point of load, and a surrounding zone of tension, as shown in Figure 2.1. The compressive membrane forces surrounding the load increase the flexural capacity of the slab. This membrane action exists even if supports are not restrained; the magnitude of such in-plane forces is higher for slabs whose edges are restrained.

Recently, some have attempted to utilize the increased capacity of slabs due to arching action in the design of highway bridge decks. In the mid-1970's, the Ontario Ministry of Transportation and Communications adopted a code that allowed for the empirical design of bridge decks. This empirical design, based on survey data from actual bridge loadings, requires an isotropic reinforcing layout that uses much less steel than current AASHTO design procedures. Much research has been conducted testing this procedure, and many actual bridges have been built using this design method, and subsequently performed satisfactorily.

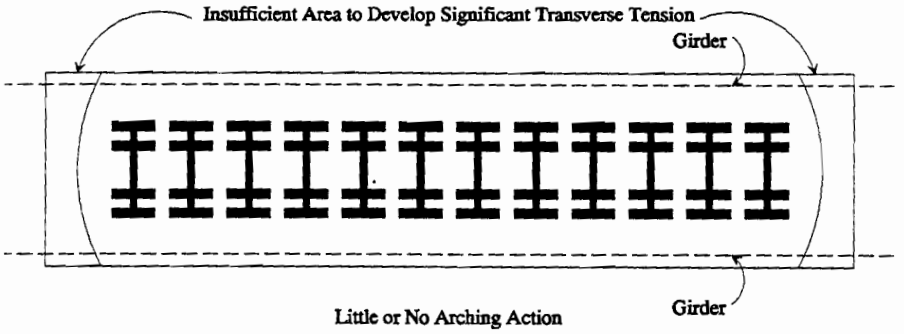

Figure 2- 2 Lack of arching action in slab subjected to closely spaced axles

Another question about arching action is how its behavior is affected when the load is applied in more than one place. As mentioned before, a point load creates the effect of a flat dome in a concrete slab. However, little is known about how a line load or a group of closely spaced loads might affect this dome-like behavior. This is a practical concern in bridges when dealing with long, multi-axle trailers carrying unusually large loads. In the point-load scenario, the "dome" is created by a central compression zone, balanced by a surrounding tension ring. If this tension ring is also loaded, it will go into compression, causing the tension zone to spread toward the supports, as shown in Figure 2.2. This "spreading" of the dome reduces the effectiveness of the arching action.

2.3 FATIGUE BEHAVIOR OF BRIDGE DECKS

Under cyclic stresses, a material's load-carrying capacity can deteriorate – the higher the number of cycles, the greater the deterioration. If a material is subjected to a large number of loading cycles, its ultimate capacity can decrease, even if the level of load is fairly small relative to the ultimate value. This phenomenon, referred to as fatigue deterioration, is of particular concern in the design of highway bridges and bridge decks. These structures are subjected to millions of loading cycles over their design lives, sometimes at very large loads relative to the loads assumed for design purposes.

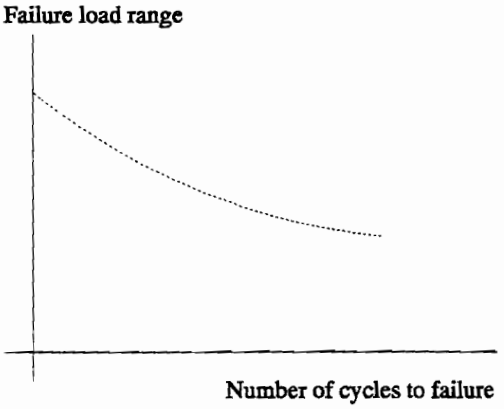

Figure 2- 3 Example of S-N curve

To predict the reduction in the capacity of a fatigued structure, one must establish a relationship between the relevant stress range and the number of stress cycles. This relationship is typically known as an "S-N curve." An example of an S-N curve is shown in Figure 2.3.

On an S-N curve, the zero-cycle point is merely the static capacity of the slab, and is relatively easy to predict through analysis and testing. However, the rest of the curve is less well known, and finding points through experimental tests is an important goal of this project. For real bridges, fatigue cycles can be estimated as a function of traffic and

age, and these experimental S-N curves can then be related, through analytical models, to the reduced capacity of the real bridges.

Two types of fatigue will be studied in this project: pulsating fatigue, which concerns a constant-location, varying-magnitude load; and rolling fatigue, which concerns a constant-magnitude, varying-location load.

Research on fatigue strength of slabs was conducted by Japanese to compare the results from rolling fatigue loads to those from pulsating fatigue loads [12]. For rolling fatigue tests, they developed the fatigue testing machine simulating a running wheel load with a moving range of 200 mm (7.9 in.). Two different sets of slabs, one for small scale and the other for full scale, were tested. The full scale slabs were 3 m (9.8 ft) long, 2 m (6.6 ft) wide, and 19 cm (7.5 in.) thick. The slabs were supported along the longitudinal sides, and elastically supported at the other two sides by crossing beams. Four corners of the slabs were restrained against uplift.

The slabs were indeed failed by punching shear, and S-N curves were obtained. The S-N curves for rolling fatigue loads dropped to about a half of those obtained under the pulsating fatigue loads. They also concluded that the fatigue capacity of the slabs was mainly governed by the torsional moments and shear forces in slabs.

In their report, though, it was unclear how the moving range of the loads or the size and shape of the loaded area were determined, which are believed to be the main factors affecting the results of rolling fatigue tests. Also, it was not clear what load range for pulsating fatigue tests was used to compare the results from the pulsating fatigue tests with those from the rolling fatigue tests.

2.4 PREVIOUS RESEARCH OF PROJECT 1305

The design of the bridge specimen was carried out [1]. The finite element model representing the experimental slab specimen was analyzed using a sequential linear analysis as explained in the next chapter. The configuration of the slab and the loading pattern is shown in Fig. 2.4.

Two important characteristics were studied in the finite element model. First, the model was analyzed for general arching action behavior. The expected arrangement of a central compression surrounded by a tension ring was confirmed. Element stress analysis confirmed general punching shear behavior. Also, the model confirmed that the arching action is even present in slabs that do not have lateral-resistant supports.

Another important factor needed from the analytical model pertained to the rolling fatigue test. It was necessary to know how much lateral movement of the rolling load was needed to produce the desired stress range in the specimen; that is, the minimum

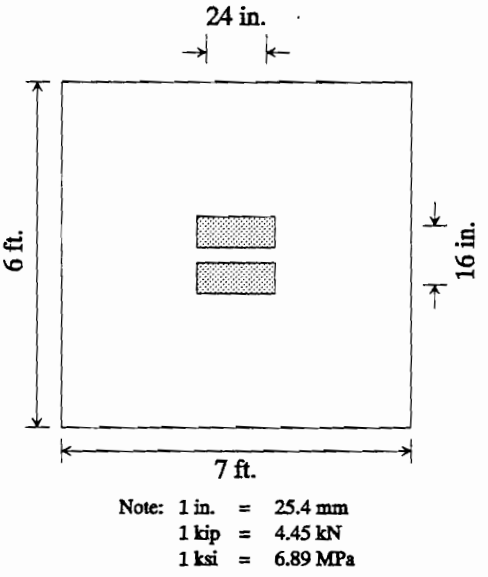

Figure 2- 4 Plan view of loading pattern for specimen model

movement of the load necessary for the maximum tensile stress perpendicular to the failure plane to go from the cracking tensile stress to a compressive stress. The necessary movement was found to be 18 inches (457 mm).

Based on this analytical result, a test setup for static loading, pulsating fatigue loading, and rolling fatigue loading was developed and implemented. The static test was performed and showed a punching shear failure pattern incorporating arching action.

CHAPTER THREE

ANALYTICAL MODEL

3.1 GENERAL

Because of the time and expense required to build a full-size bridge deck, it was considered important to develop analysis procedures to obtain a appropriate laboratory specimen that would represent only a part of the full-size bridge deck and yet simulate the exact behavior of the entire deck. The real-world bridge deck and test specimen were analyzed using a sequence of linear elastic analyses using SAP90, a widely used microcomputer structural analysis program [16].

At the first phase of structural analysis, models for the full-size bridge and experimental specimen were compared as described in detail in the previous report [1]. Two important results were obtained from these finite element analyses:

1) Arching action in cracked slab existed and was observable in both models, even those without lateral restraint of external supports.

2) For the rolling fatigue tests, the load needed to move a total 18 inches (457 mm) in order for the failure surface to experience the full stress range of tension and compression.

Based on these previous results, a more refined model was developed.

3.2 REFINED MODELING OF THE CRACKED BRIDGE DECK

The specimen was modeled using a finite element mesh consisting of 8-node isoparametric solid elements. Each node had three displacement degrees of freedom and no rotational ones. Stresses at the center of the element were obtained, as well as displacement, reactions and forces at nodes. In the refined analysis, a total of 3150 solid elements was used instead of the 1344 elements used previously, permitting greater accuracy. Because of symmetry of geometry and load configuration, only half of the slab was modeled. The model is shown in Figure 3.1.

Since the finite element program SAP90 used for the study was designed to analyze a linear elastic model, a sequential linear analysis procedure was adopted to accommodate the cracking behavior of concrete bridge decks. Basic concepts were explained in previous TxDOT research [2], and are reviewed here.

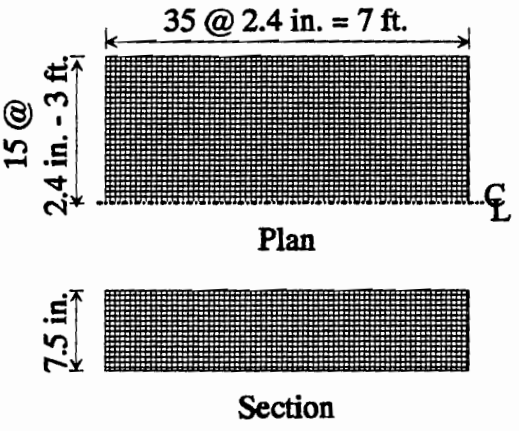

Figure 3- 1 ***Refined finite element model for the half specimen.***

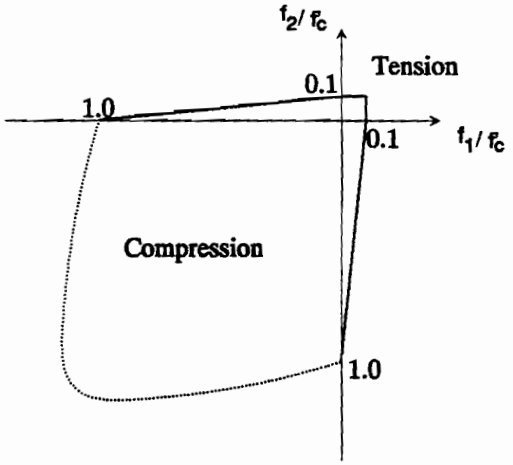

Figure 3- 2 ***Kupfer's biaxial stress criterion***

A small load was applied to the specimen and the stresses at the center of each element were examined whether they reached the cracking value for concrete. The tensile cracking stresses were set to 10 percent of f°c based on Kupfer's biaxial failure envelope as shown in Fig. 3.2 [22]. If the stress exceeded this value, the entire element was treated as cracked perpendicular to the direction of that stress. This technique, known as the smeared cracking approach, assumed that the cracked concrete remained continuous, and the cracks were distributed throughout the cracked element. The stiffness of the element was then set to zero in the direction perpendicular to the cracked plane. The plane-stress constitutive matrix for concrete cracked perpendicular to the x axis is as shown in Eq. 3.1:

$$\begin{bmatrix} \sigma_x \\ \sigma_y \\ \tau_{xy} \end{bmatrix} = \begin{bmatrix} 0 & 0 & 0 \\ 0 & E_c & 0 \\ 0 & 0 & 0 \end{bmatrix} = \begin{bmatrix} \varepsilon_x \\ \varepsilon_y \\ \gamma_{xy} \end{bmatrix} \qquad [3.1]$$

To prevent numerical difficulties, a reduced shear modulus was incorporated. A reduction factor β of 0.5 was used along with a shear modulus G, representing the remaining shear stiffness in the cracking plane due to the aggregate interlock and dowel action. The tensile stiffness of reinforcement crossing the cracked plane was also included, as shown in Eq. 3.2:

$$\begin{bmatrix} \sigma_x \\ \sigma_y \\ \tau_{xy} \end{bmatrix} = \begin{bmatrix} \rho_{eff} & E_s & 0 \\ 0 & E_c & 0 \\ 0 & 0 & \beta G \end{bmatrix} \begin{bmatrix} \varepsilon_x \\ \varepsilon_y \\ \gamma_{xy} \end{bmatrix} \qquad [3.2]$$

$$\rho_{eff} = \frac{A_s}{bt}$$

where, ρ_{eff}: effective tensile steel ratio perpendicular to the cracking plane

A_s: area of reinforcement perpendicular to the cracking plane

b: width

t: depth of the element

In summary, this smeared cracking model idealized cracking reinforced concrete as an orthotropic material, with reduced tensile stiffness perpendicular to the cracking orientation, and reduced shear stiffness parallel to it.

This smeared cracking model was extended to three dimensions. The flexibility matrix is shown in Eq. 3.3 for the case of cracking perpendicular to the x axis:

$$\begin{bmatrix} \varepsilon_x \\ \varepsilon_y \\ \varepsilon_z \\ \gamma_{xy} \\ \gamma_{yz} \\ \gamma_{yz} \end{bmatrix} = \begin{bmatrix} \frac{1}{\rho_{eff} E_s} & 0 & 0 & 0 & 0 & 0 \\ 0 & \frac{1}{E_c} & -\frac{\nu}{E_c} & 0 & 0 & 0 \\ 0 & -\frac{\nu}{E_c} & \frac{1}{E_c} & 0 & 0 & 0 \\ 0 & 0 & 0 & \frac{1}{\beta G} & 0 & 0 \\ 0 & 0 & 0 & 0 & \frac{1}{G} & 0 \\ 0 & 0 & 0 & 0 & 0 & \frac{1}{\beta G} \end{bmatrix} \begin{bmatrix} \sigma_x \\ \sigma_y \\ \sigma_z \\ \tau_{xy} \\ \tau_{yz} \\ \tau_{zx} \end{bmatrix} \qquad [3.3]$$

The sequential linear analysis was then continued by applying an incremental load until more elements reached the cracking criterion. Those elements were modified with a smeared cracking stiffness, and the process was repeated. The total stiffness of the structure would decrease as more elements were cracked, as shown in Figure 3.3. This gave the dashed envelope curve a nonlinear shape, with a decreasing slope.

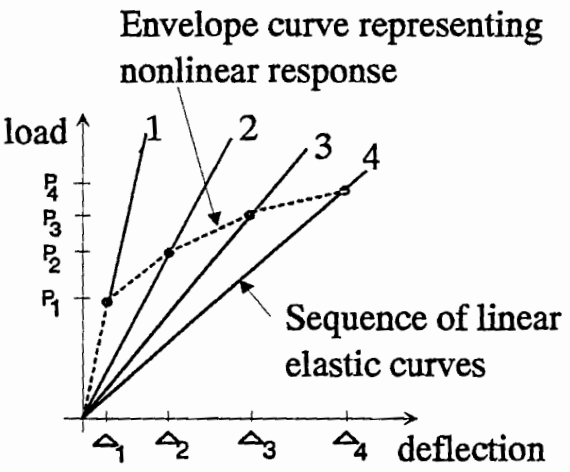

Figure 3- 3 Load-deflection curve using sequential linear analysis

3.3 MODEL FOR STATIC AND PULSATING FATIGUE TESTS

Due to the symmetry, a half of the 6 feet (1.83 m) wide, 7 feet (2.13 m) long, and 7½ inches (191 mm) thick specimen was modeled. It was consisted of the solid elements of 15 by 35 in plan and of 6 layers in section, a total of 3150 elements. The uniformly distributed load was simulated using equivalent concentrated nodal loads. The pseudo-nonlinear approach described in previous section was used, and nonlinear load-deflection curve was developed.

Finding the stresses on concrete and reinforcement was an important aspect of the program. As explained throughout the report, those stresses were used to compare the analytical model to the test results and also used to confirm the analytical assumption. A manipulation was done to find the calculated reinforcement stresses from the output stresses of SAP90. For the cracked elements, the corresponding reinforcement stresses were obtained by multiplying the output stresses by n/ρ_{eff}, where n was the modular ratio and ρ_{eff} was the effective steel ratio. For the uncracked elements, the reinforcement stresses were obtained by multiplying the output stresses by n.

3.4 MODEL FOR ROLLING FATIGUE TESTS

The same sequential linear procedure for static and pulsating fatigue tests was used again to predict the behavior of the specimen under rolling load. The only difference was the load location. As noted in Ref. [1], the optimum movement of the load was 18 inches (457 mm). A finite element analysis was carried out with a load located 9 inches (229 mm) from the slab center.

One concern in developing the rolling fatigue setup was whether the forces on the roller skids would remain constant as the skids moved back and forth, because of the complexity the load delivered. The load was applied on the rods at each ends of the frame and released. The rods then delivered the forces to the skids on top of the slab through the top girder, which tied the rods. Then the skids moved back and forth 9 inches (229 mm) (see details in the following chapter). Thus, before the actual test, it was unknown whether the forces on the skids would remain constant. A finite element analysis was conducted to see the variation of forces on rods and skids; it showed that the forces on the skids remained almost constant. These analytical results were compared to the experimental results as explained in Chapter 7.

CHAPTER FOUR

DEVELOPMENT OF TEST SETUP

4.1 INTRODUCTION

The main subjects on this chapter are as follows:

- design of test specimen
- test procedure for each test: static, pulsating fatigue, and rolling fatigue
- design of test frame
- instrumentation
- data acquisition system
- servo-controller system

4.2 TEST SPECIMEN

As discussed in the previous chapter, the size of the test slab was determined by extensive finite element modeling, so that the selected experimental specimen would behave like real-world bridge decks. The specimens were reinforced concrete slabs, 6 feet (1.83 m) wide, 7 feet (2.13 m) long, and 7½ inches (191 mm) thick.

One of the main purposes of this project is to observe the characteristics of punching shear behavior in fatigue of concrete bridge decks. To make sure that the slabs would fail in punching shear, several other possible failure mechanisms were reviewed, including flexural failure, bond and development failure, or direct shear failure. Yield line theory suggested that a normal reinforcement layout based on AASHTO design codes for bridge decks would be insufficient to prevent flexural failure under extreme overloads. Thus, the required bottom flexural reinforcement was about three times the amount typically used in highway bridges. The experimental specimen, representing only a part of a bridge deck, was not continuous over the supports, and therefore did not provide sufficient development length for flexural reinforcement. Thus, 180-degree hooks on bottom bars were required to prevent pull-out failure. Also, the cover was increased to 2½ inches (64 mm) to prevent concrete splitting. To prevent direct shear failure, it was required that the slabs be supported inside of the end of the hook. This kept the side cover from shearing off due to concentrated loads on the edge of the slab. ASTM A615, Grade 60 reinforcing bars (#4, #5, and #6) were used. A typical reinforcement layout is shown in Figure 4.1.

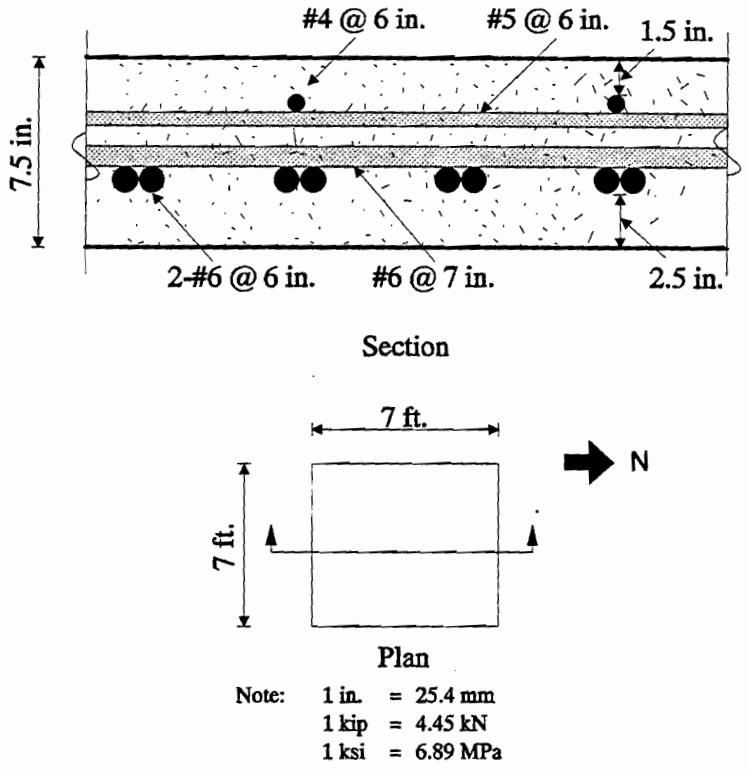

Figure 4- 1 Reinforcement layout

Concrete used for the tests was TxDOT Type S [20]. Due to the heavy reinforcement layout, the maximum coarse aggregate was _ inch (9.5 mm) to enhance workability. Material characteristics and cylinder strength of concrete are given in Appendix A.

Formwork for three slabs was built, permitting the casting of three slabs at once.

4.3 TEST FRAME

Since this research project was attempting to test specimens representing parts of full-scale bridge decks, very large loads would be necessary to fail the specimens in the desired fashion. To place such large loads on the slabs, a very stiff and strong steel reaction frame was necessary.

Fatigue was also an important consideration in the design of the reaction frame itself. Because the specifications called for moving and rolling fatigue tests involving large loads and many cycles, it was crucial that the tests would fatigue and fail the specimens, and not the testing frame. Another concern with fatigue tests was time. Many of the fatigue tests would require over a million cycles, and each test might require several weeks. To increase the efficiency of testing, two frames were designed, one for static or pulsating tests, and the other for rolling tests.

The steel frame consisted of A36 rolled steel shapes, primarily wide flange (W12 and W14) for girders and beams, and channel sections (C12) for columns. Angles and A325 bolts were used for connections. Welds were avoided wherever possible, due to concern over the fatigue performance of welded connections.

Detailed descriptions for three different test setups are given in the following sections.

4.4 TEST SETUP FOR STATIC TESTS

A schematic drawing of the testing frame for static tests is shown in Figure 4.2. The frame consisted of columns made up of four channel sections at both south and north sides, and of a top girder consisting of two W14 rolled sections and two 1-inch-thick (25.4 mm) plates. Each side of the slab was supported on a W12 section, and these four beams in turn rested on four more W12's lying transverse to the slab. The four bottom beams' primary purpose was to

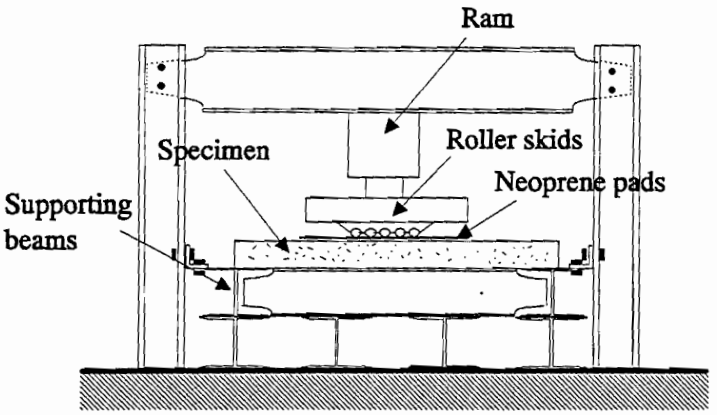

Figure 4- 2 Test setup for static tests

elevate the slab and its support, in order to provide access to the underside of the slab. This was necessary in order to apply external concrete strain gages, as well as to observe cracking patterns during testing. Also, a limit switch, to shut off the servo-controller in case of excessive displacement, could be installed underneath the slab for fatigue tests.

A 400-ton (3560 kN) capacity hydraulic ram was attached to the top girder. For static tests, load was applied through the ram by applying hydraulic pressure with a hand pump. The load was delivered to the slab through two heavy-duty roller skids attached to the web of a W27 lying on its side. Between the steel roller skids and the slab was a ½-inch-thick (12.7 mm) sheet of 70-durometer neoprene, which protected the slab from localized damage, and simulated the contact between rubber tires and concrete. After the first static test, neoprene pad was replaced with a pair of _-inch-thick (15.9 mm) steel plates sitting on top of hydrostone. Its function, to apply equal force from the ram to two separate footprints, remained the same.

The load was monitored by a load cell in contact with the ram, as well as by a pressure transducer attached to the hand pump. Displacement of the slab was recorded using a linear potentiometer. Strains in both concrete and reinforcing steel were monitored using electrical-resistance strain gages. All information was recorded using a Hewlett-Packard scanner and a microcomputer.

4.5 TEST SETUP FOR PULSATING FATIGUE TESTS

As the test setup for pulsating tests was very similar to the static tests, the same frame was used. The main difference was how to control the loading. Pressure was applied to the ram using an electric pump. The flow of the pump was controlled by an MTS servo-controller, which in turn regulated a servo-valve and line-tamer. The controller monitored maximum and minimum loads, and counted the number of cycles applied to the specimen. It also checked for any large variations in load or excessive displacement by a mechanical limit switch, and therefore shut the system down in case of failure or error. A schematic drawing of the closed-loop servo-controlled system is shown in Figure 4.3.

In these tests, the rate of loading was dependent on how quickly hydraulic oil could be pumped in and out of the ram. With the initial test setup, the maximum flow rate was consistent with a loading frequency of about 0.15 Hz for a 50-kip (222.5 kN) load range. A 300-ton (2670 kN) ram replaced the existing 400-ton (3560 kN) ram. Fittings on the ram were re-ported from _ to 1 inch (from 9.5 mm to 25.4 mm) diameter. This increased the loading frequency to about 1 Hz for a 140-kip (623 kN) load range.

After the static tests, a few other modifications made on testing setup. Roller skids and W27 beam were replaced with a 3-inch-thick (76.2 mm) steel plate (14" by 24" (356 mm by 610

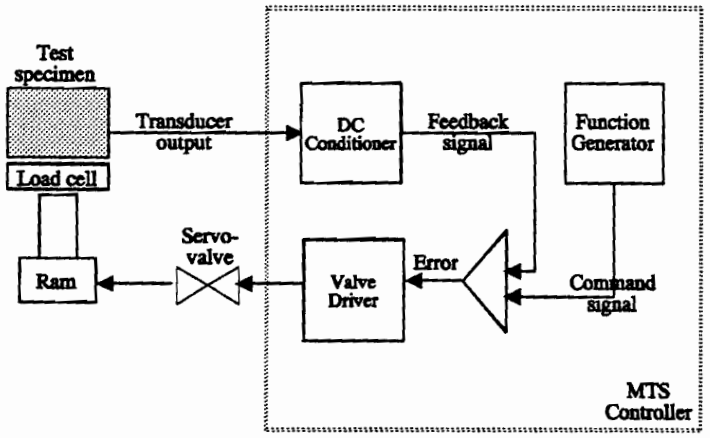

Figure 4- 3 Closed-loop servo-controlled system

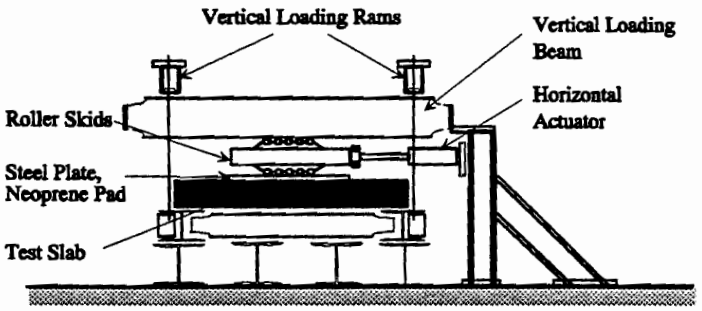

Figure 4- 4 Test setup for rolling fatigue tests

mm)). A pair of steel plates, in contact with this thick plate, rested on the ½-inch-thick (12.7 mm) neoprene pad, instead of on the hydrostone used in second static test. These modifications, again, did not affect the way force was delivered to the specimen from the ram.

4.6 TEST SETUP FOR ROLLING FATIGUE TESTS

The test setup used for rolling fatigue tests (Figure 4.4) resembled the setup used in the pulsating tests (Figure 4.2), with a few modifications. The only change in the frame involved moving down the top girder until it rested on the loading apparatus, which now consisted of four roller skids – two on the bottom and two on the top of the W27 beam.

The top girder was then loaded downward by four matched rams on top of the girder. These rams were connected to a common hydraulic manifold so that equal force could be applied to each of them. Each ram applied the load through a pair of rods connecting the ram to the bottom beams supporting the slab. This produced a compressive load through the roller skids, which loaded the slab with the footprint caused by the two skid treads. A ½-inch-thick (12.7 mm) sheet of neoprene was used to protect the concrete from any wear caused by the steel skids.

After the initial load was applied using the top rams, the rams were closed off. The rods were tied to the frame by tieing down the bolts on top of the girder, maintaining the load in the vertical rods, and pressure was released. Then, to obtain rolling action, the skate was rolled back and forth by a horizontal ram connected to the column tied to the floor. As mentioned in previous chapters, the total moving range was 18 inches (457 mm). For fatigue loading, the horizontal ram was connected to a servo-controller and was controlled by a displacement function. The number of rolling cycles was then monitored in the same way as the pulsating cycles, as described in the preceding section.

Although extensive work was conducted on the rolling fatigue setup, the apparatus was still not operating successfully at dynamic loading rates. A detailed description of this is given in Chapter 7.

CHAPTER FIVE

RESULTS OF STATIC TESTS

5.1 DESCRIPTION OF STATIC TESTS

In this chapter, results and observations from static tests are presented. The first priority in the series of tests was to obtain the punching shear capacity for static tests. This would then be considered the zero-cycle ordinate on the S-N curves; the pulsating fatigue tests would supply other data points at different numbers of loading cycles. Data acquired from the tests were also used to verify the analytical predictions made in the beginning of program.

Tests on two cast-in-place concrete slabs were conducted. The load-deflection relationship, local stresses and cracking pattern of specimen, and performance of test frame were observed and monitored.

The results of the first static test were reported in detail in the previous report [1]. The ultimate load capacity was 173 kips (770 kN); as desired, failure was by punching shear. The second test was followed by a few modifications on test setup as described in the preceding chapter.

5.2 RESULTS FROM SECOND STATIC TEST

The deflection of the slab was measured using a linear potentiometer at the center of top surface on the slab, whose output was subtracted from the average output of two linear potentiometers at the ends of the slab. In other words, the measured deflection was the vertical midpoint deflection of the specimen, relative to the ends of slab. This measurement procedure was adopted in order to isolate the slab behavior itself, and to eliminate the effects of any frame deflection or support uplift. The load was applied monotonically through the 400-ton (3560 kN) ram and a hand pump, and was monitored using a load cell on top of roller skids, as well as a pressure transducer on the hand pump. The load-deflection curve for the second static test is shown in Figure 5.1.

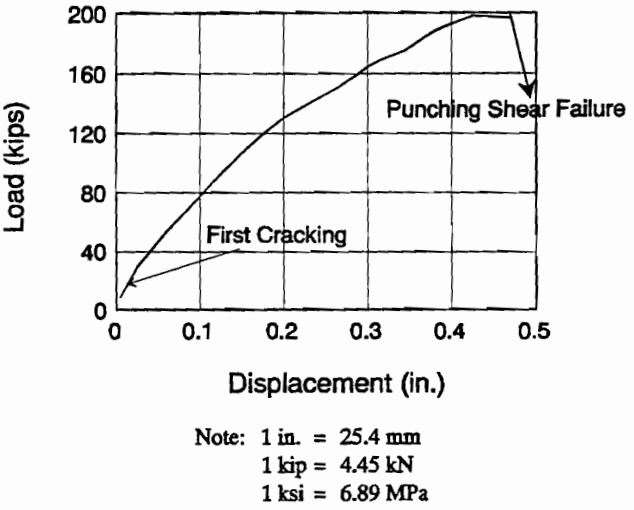

Figure 5- 1 ***Load-deflection relationship (second static test)***

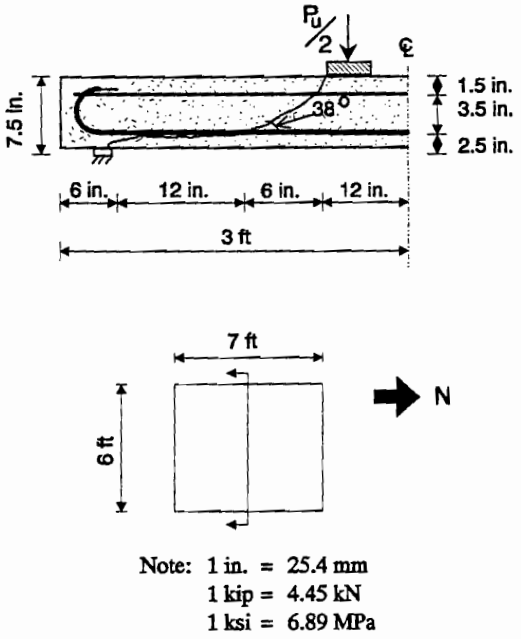

Figure 5- 2 Cross section of failed specimen (second static test)

Prior to the second static test, a trial fatigue test was conducted to find suitable loading rates for a given test setup. The maximum load imposed on the specimen was about 100 kips (445 kN) at 0.15 Hz. During this trial test, first cracking was observed at the bottom of slab at the load of 18 kips (80.1 kN); it progressed in both directions as load increased. As shown in the static load-deflection curve of Figure 5.1, recorded after this trial fatigue test, the load-deflection relationship was linear up to about 100 kips (445 kN), and then showed a slight decrease in slope. Sudden failure was observed when the static load reached 205 kips (912 kN), at a slab deflection of 0.48 inches (12.2 mm). The failure mode was punching shear, associated with the formation of a truncated pyramid in the middle of the slab. The failure surface formed in the specimen until it reached the bottom reinforcement; cracks then propagated toward the supporting beams. A cross section of the failed specimen is shown in Figure 5.2. The failure pattern was quite similar to that of the first static test, although the ultimate failure load was 18% higher. Taking possible experimental scatter into account, this variation was believed to be acceptable. While the flexural cracks propagated in both directions, wider cracks were observed in the east-west (transverse) direction.

5.3 LOCAL STRESSES FROM SECOND STATIC TEST

Data for strains in concrete and reinforcing steel were collected during the test. Ten internal strain gages were installed on the surface of reinforcement, and five external gages were installed on the bottom surface of the slab. Strain values were then converted to the corresponding stresses. Stresses versus load relationship for top and bottom bars are shown in Figures 5.3 and 5.4 respectively.

Only six out of ten steel gages were available for the investigation; the remaining steel gages and all the concrete gages were damaged. As shown in Figure 5.3, top-bar stresses in the longitudinal direction ranged from 9 ksi (62.0 MPa) to 22 ksi (151.6 MPa) in compression, and top-bar stress in the transverse direction was 2 ksi (13.8 MPa) in tension for 150-kip (668 kN) loading. On bottom bars, only one longitudinal gage was available, whose stress was 33 ksi (227 MPa) at 150 kips (668 kN). Gages in the transverse direction showed 20 ksi (138 MPa) and 25 ksi (172 MPa) compressive stresses at that same load, as shown in Figure 5.4.

Every gaged reinforcing bar had tensile stress, except the top transverse bar. This indicated that the cracking had propagated more than 5 inches (127 mm) from the bottom of specimen, putting some of top bars as well as bottom bars in a tensile zone. This was confirmed by the analytical model discussed in the following section. Another observation was

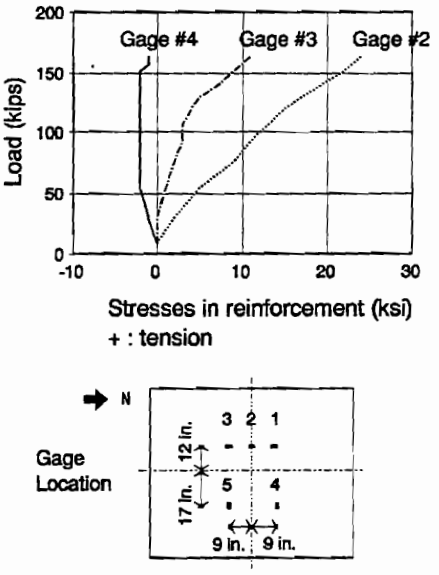

Note: 1 in. = 25.4 mm
1 kip = 4.45 kN
1 ksi = 6.89 MPa

Figure 5- 3 Stresses vs. load on top reinforcement (second static test)

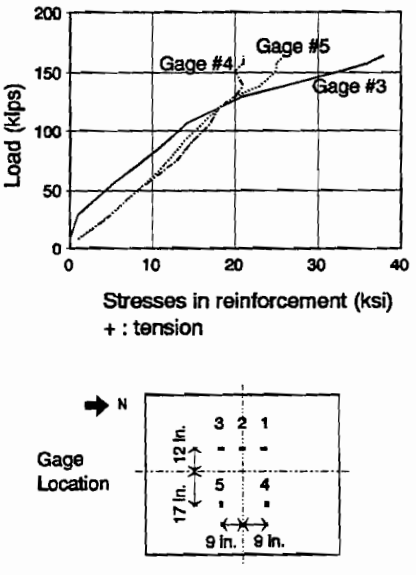

Note: 1 in. = 25.4 mm
1 kip = 4.45 kN
1 ksi = 6.89 MPa

Figure 5- 4 Stresses vs. load on bottom reinforcement (second static test)

that stresses in reinforcement were far below the specified yield strength of 60 ksi (413 MPa). It showed that the large amount of reinforcement prevent flexural yield of reinforcing bars, as desired.

5.4 ANALYTICAL VERIFICATION

5.4.1 Analytical Verification of Slab Capacity

Four different analytical procedures were used to predict the capacity of the tested specimens: yield-line theory was used for a flexural capacity; an ACI equation, an AASHTO equation and a general punching shear model were used to estimate punching shear capacity. The previous report [1] described those analytical models in detail. The experimental capacity of specimens is compared to those predicted capacities in Figure 5.5. Experimental capacity was slightly higher than predicted punching shear capacity from a general model. ACI and AASHTO codes underestimated the capacity, mainly because those codes neglected the beneficial effect of arching action in the cracked slab. These static test results were later used to develop S-N curves for the fatigue characteristics of the cast-in-place deck.

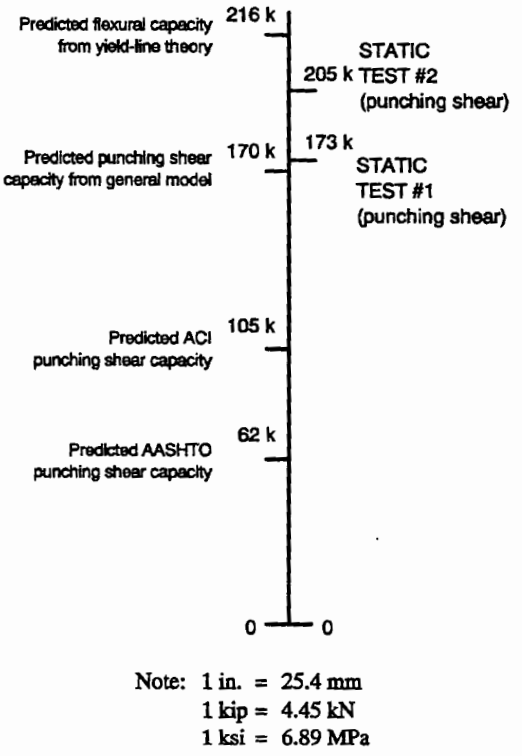

Figure 5- 5 Slab capacity (predicted vs. measured)

5.4.2 Analytical Verification of Local Stresses

From the beginning of the research program, the analytical model was of great importance as a means to represent the bridge deck using a experimental specimen. One aspect of the verification involved comparing measured local stresses in reinforcement to those obtained from the analysis. Detailed procedures to obtain predicted stresses are discussed in Chapter 3 of this report.

Stresses were compared at two different loading stages, 92 kips (409 kN) and 150 kips (668 kN), for transverse and longitudinal reinforcing bars. As shown in Figures 5.6 through 5.9, the measured results generally agreed well with the analytical predictions. In Figures 5.7 and 5.9, stresses on longitudinal reinforcement were compared at 92 kips (409 kN) and 150 kips (668 kN), respectively. The tensile stresses were predicted in both top and bottom bars; the actual reading was higher than predicted, especially at the higher load of 150 kips (668 kN). The widespread flexural cracks perpendicular to the longitudinal direction corroborated these results. This was believed due to a uplifting force on end columns connected to the supporting frame, which might cause higher stresses on reinforcement running between two columns than predicted ones. Observed compressive stresses on top bars in transverse direction were also predicted by the finite element model as shown in Figures 5.6 and 5.8, and predicted bottom

bar stresses in this direction matched well with the measured ones. As there were only a few gages to compare, however, it is recommended that more strain gages be installed for analytical verification during future tests.

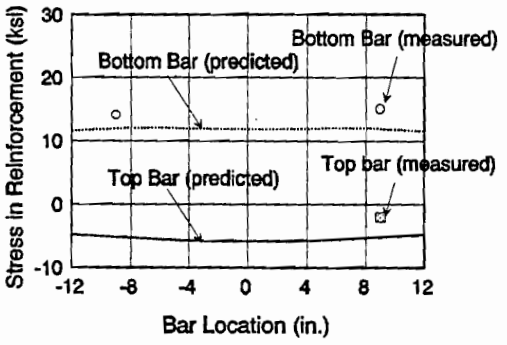

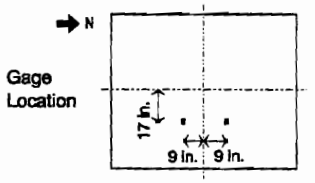

Note: 1 in. = 25.4 mm
1 kip = 4.45 kN
1 ksi = 6.89 MPa

Figure 5- 6 Stress comparison in east-west direction (P = 92 kips), second static test

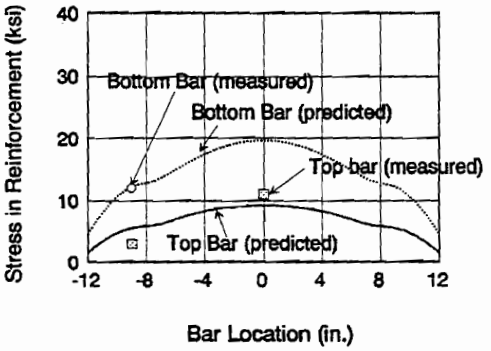

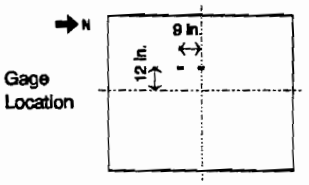

Note: 1 in. = 25.4 mm
1 kip = 4.45 kN
1 ksi = 6.89 MPa

Figure 5- 7 Stress comparison in north-south direction (P = 92 kips), second static test

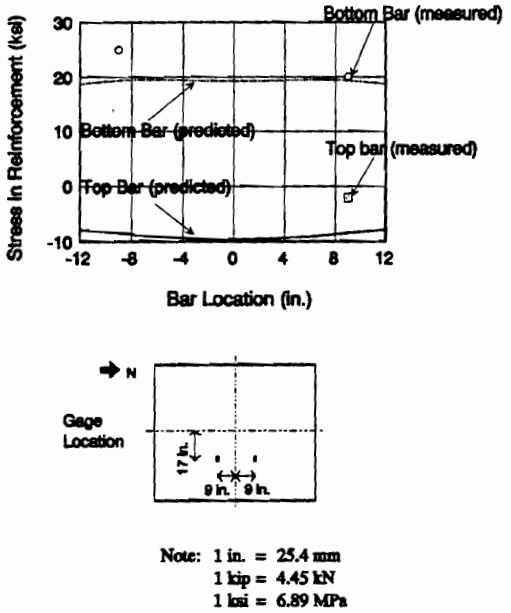

Note: 1 in. = 25.4 mm
1 kip = 4.45 kN
1 ksi = 6.89 MPa

Figure 5- 8 Stress comparison in east-west direction (P = 150 kips), second static test

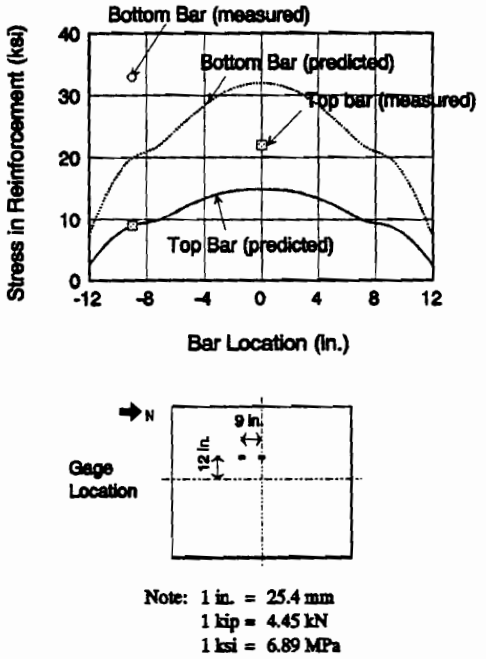

Note: 1 in. = 25.4 mm
1 kip = 4.45 kN
1 ksi = 6.89 MPa

Figure 5- 9 Stress comparison in north-south direction (P = 150 kips), second static test

CHAPTER SIX

RESULTS OF PULSATING FATIGUE TESTS

6.1 DESCRIPTION OF TESTS

The main purpose of the pulsating fatigue tests was to develop S-N curves for concrete bridge decks failed by punching fatigue. The ultimate static capacity of specimens was used for the zero-cycle ordinate on the S-N curve; pulsating test results would give some data at other load ranges. The following chapter describes the results of the pulsating fatigue tests carried out to date.

As the first phase of pulsating fatigue tests, an investigation was conducted to determine what load range or maximum load would be imposed upon the specimen. It was required that the load range for first test be high enough to fail the slab at a few cycles, but not at a single cycle, as in a static test. Based on this, the maximum load was set at no more than 85 percent of the failure load, estimated by a general punching shear model. The minimum load was set at about 10 percent of maximum load, typical for general fatigue tests on concrete. Thus, the load range for the first series of pulsating fatigue tests was 130 kips (579 kN) (between 15 and 145 kips (66 kN and 645 kN)).

Another important characteristic for fatigue tests were to develop an adequate cycling speed. Previous experimental research indicated no significant difference in fatigue life for frequencies between 0.5 Hz and 7.5 Hz [21,23,24]. Based on trial tests, a frequency of 1 Hz was selected for the given test frame.

The same frame used for static tests was again used after a few modifications. Instrumentation and data acquisition system for the tests are described in detail in Chapter 4.

6.2 RESULTS FROM PULSATING FATIGUE TESTS

Three concrete slabs were tested, designated S1P145, S2P145, and S3P145 respectively. The material characteristics are given in Appendix A. The compressive strength of concrete was 6200 psi (42.7 MPa), slightly higher than the strength used in static tests. Considering that the ultimate capacity of slab is a function of tensile concrete strength, which is proportional to the square root of compressive concrete strength, this difference in concrete compressive strength is considered negligible.

Test results are summarized in Table 6.1. Load-deflection curves for each specimen are given in Figures 6.1, 6.2, and 6.3 respectively.

Table 6- 1 ***Summary of pulsating fatigue tests (load range: 130 kips)***

Specimen	Test Date	Cycles to Failure	Comments
S1P145	3/16/94	1,443	rapid failure (10 cycles)
S2P145	3/30/94	29,581	slow failure (1500 cycles)
S3P145	4/6/94	6,019	rapid failure (10 cycles)

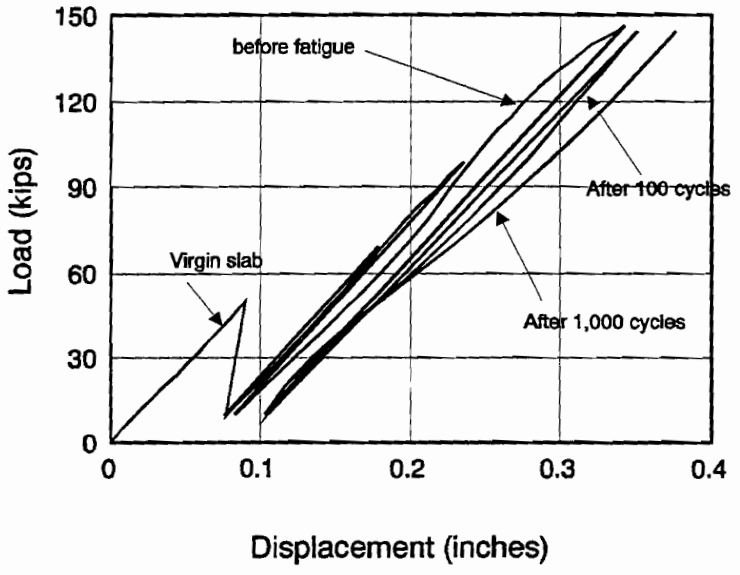

NOTE: 1 in. = 25.4 mm
1 kip = 4.45 kN
1 ksi = 6.89 MPa

Figure 6- 1 ***Static load vs. deflection for first pulsating fatigue specimen (S1P145)***

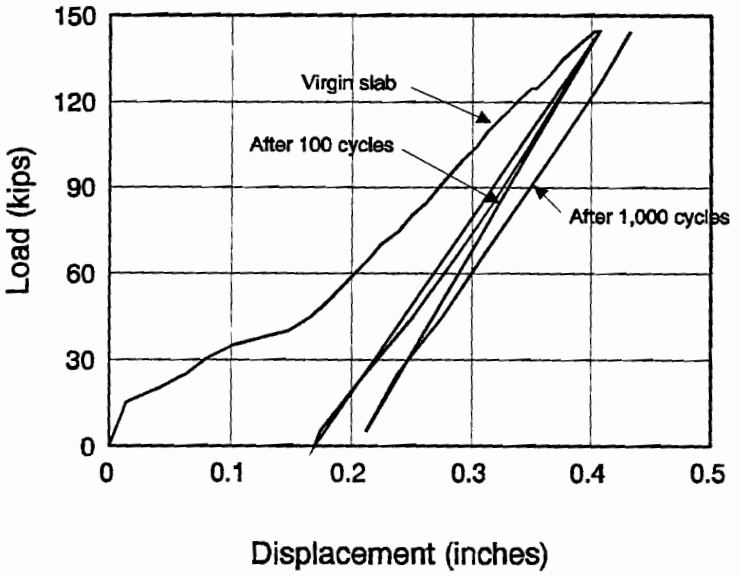

NOTE: 1 in. = 25.4 mm
1 kip = 4.45 kN
1 ksi = 6.89 MPa

Figure 6- 2 Static load vs. deflection for second pulsating fatigue specimen (S2P145)

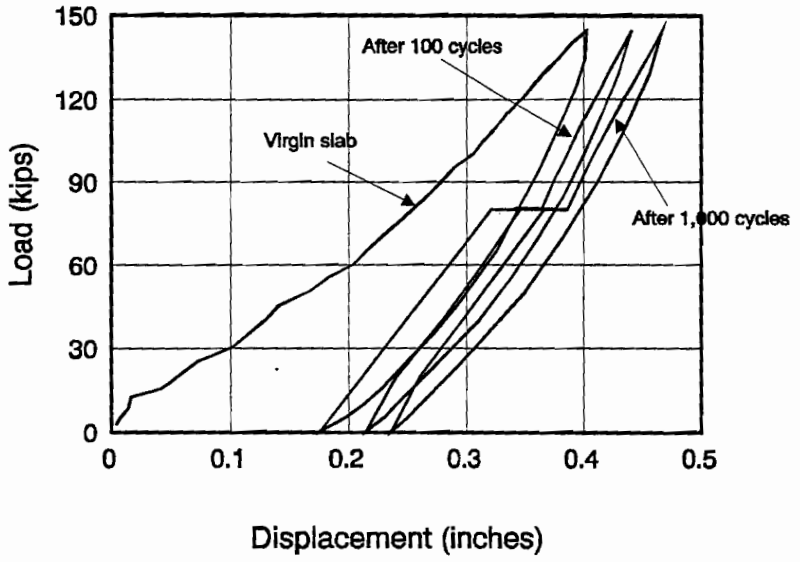

NOTE: 1 in. = 25.4 mm
1 kip = 4.45 kN
1 ksi = 6.89 MPa

Figure 6- 3 Static load vs. deflection for third pulsating fatigue specimen (S3P145)

6.2.1 *Results of Pulsating Fatigue Tests for Specimen S1P145*

The first specimen (S1P145) was loaded statically to 50 kips (223 kN) and unloaded. A 100-kip (445 kN) load was then applied to monitor overall frame stability and controller response on a smaller load range, rather than over the full range of 130 kips (579 kN). After this pre-loading, the slab was loaded up to 145 kips (645 kN) statically, followed by cyclic loading with a load range of 130 kips (579 kN) at a dynamic rate of 1 Hz. Oil pressure was released after 100 cycles to measure the static load-deflection relation. Afterwards, cyclic load was again applied until static load-deflection data was measured at 1,000 cycles. Cyclic load was applied again until failure.

As shown in Table 6.1, Specimen S1P145 failed at 1,443 cycles by a sudden punching shear. The middle of the slab punched through along the edge of steel plates on top surface of concrete, and the bottom surface of the slab showed a distributed crack pattern, as in static tests. The limit switch, installed 1.5 inches (38 mm) below the bottom surface of the slab, triggered the emergency stop on the servo-controller and stopped the oil flow within a few cycles after formation of cracks along the edge of steel plates sitting on top of slab.

The deflection was recorded on the bottom surface of slab using a 2-inch (51 mm) linear potentiometer placed at the center of the slab. The static load-deflection relationship was monitored at 100 cycles and 1,000 cycles during dynamic loading. The results are given in Figure 6.1. The deflection at a given load increased as the loading cycles accumulated. The slab deflection at a 145-kip (645 kN) load after 100 cycles was 0.35 inches (8.9 mm), while the deflection after 1,000 cycles was 0.38 inches (9.7 mm). However, the overall load-deflection relationship in the graph is somewhat deceptive. During cyclic test with smaller load range prior to the full range test, the deflection of the slab was not recorded. As a result, the deflections in subsequent tests were measured from a deformed reference.

6.2.2 *Results of Pulsating Fatigue Tests for Specimen S2P145*

Specimen S2P145 was subjected to repeated maximum loads of 145 kips (645 kN) applied in a 130-kip (579 kN) range. The static load-deflection relationship was recorded at "virgin" slab, at 100 cycles and at 1,000 cycles. Specimen S2P145 failed at a surprisingly high number of cycles compared to Specimen S1P145. Though the same punching shear failure pattern was observed for both, the latter slab failed much more slowly. After initial cracking on the east side of the steel loading plate on the top surface of specimen, it sustained about 1500 more cycles of load, while the crack propagated around the two steel plates. The specimen finally punched through at 29,581 cycles. A schematic drawing of this sequential failure is shown in Figure 6.4.

6.2.3 *Results of Pulsating Fatigue Tests for Specimen S3P145*

The same procedure was used for Specimen S3P145. That specimen failed rapidly by punching shear at 6,019 cycles. Both specimens S2P145 and S3P145 showed similar load-deflection relationships, as shown in Figures 6.2 and 6.3. Each started to crack at about 15 kips (66.8 kN), and maximum deflection reached 0.4 inch (10.2 mm) at 145 kips

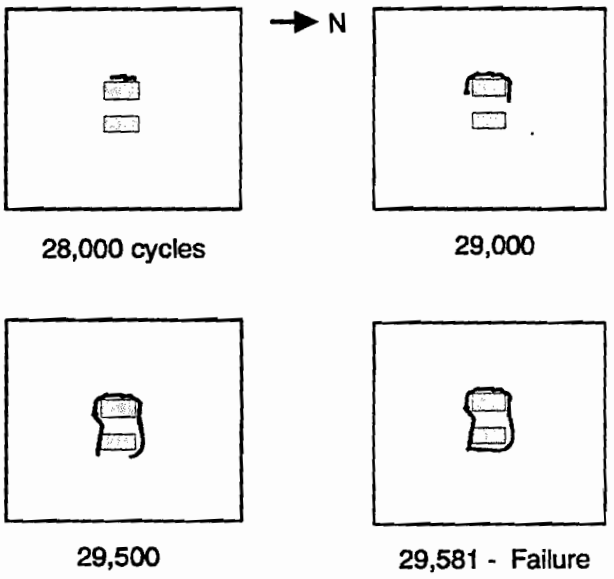

Figure 6-4 ***Failure process for second pulsating fatigue specimen (S2P145)***

(645 kN) under first monotonic static loading. The deflection after first unloading for both tests was 0.18 inch (4.6 mm). At each load the deflection increased with dynamic cycling.

6.3 S-N Curve for Pulsating Fatigue Tests

For all the pulsating fatigue tests, S-N data was plotted as shown in Figure 6.5. Ultimate capacity from the two static tests lies on the vertical axis, at 173 kips (770 kN) and 205 kips (912 kN). The three test results at 130-kip (579 kN) load range are also plotted. Generally, fatigue life is dependent on the range of the applied stress, and increases as the stress range is reduced. The dotted line of Figure 6.5 follows this basic trend. However, more test data are required to predict the S-N curve for punching shear fatigue of reinforced concrete bridge decks. A load range of 100 kips (445 kN) is planned for the next pulsating fatigue tests.

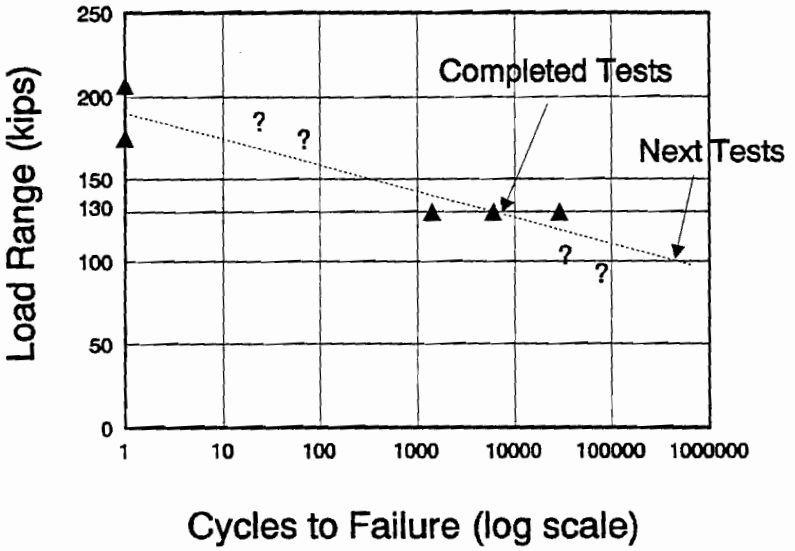

NOTE: 1 in. = 25.4 mm
1 kip = 4.45 kN
1 ksi = 6.89 MPa

Figure 6- 5 ***S-N data for pulsating fatigue specimens***

CHAPTER SEVEN

ROLLING FATIGUE TESTS

7.1 DESCRIPTION OF ROLLING FATIGUE TESTS

Pulsating fatigue tests have traditionally been the preferred method of researching fatigue effects in slabs. However, some concern has been expressed about whether such tests completely duplicate the conditions placed on highway bridge decks. Actual bridges, after all do not experience such pulsating, stationary loads. Real loadings involve loads applied by rolling vehicles. The effect of this rolling motion on the fatigue deterioration of bridge decks could be substantial, but still remains largely unknown.

The main reason that research on rolling fatigue has been rare is probably the great difficulty such experiments can cause. Experimentally, it is quite difficult to move loads large enough to fail concrete slabs, especially full-scale ones. Extensive work was conducted on the rolling fatigue test setup:

A procedure was developed to apply and maintain a constant axial load. One of the important features for rolling test setup was to maintain a constant load imposed on the specimen so that it could simulate the actual truck loading condition for the highway bridge decks. Compressive load was applied to four rams, and then a pair of calibrated rods at each ram held the load by tightening the bolts sitting on top of the girder. While roller skids moved back and forth 9 inches (229 mm) using the horizontal ram under manual control, forces on the rods were monitored. This setup demonstrated the ability to maintain a nearly constant axial load on the slab.

At the beginning of the rolling test, the rolling resistance of the roller skids was unknown, and it was impossible to install a horizontal hydraulic ram of a proper capacity to run optimized dynamic tests. A 44-kip (196 kN) capacity ram was used to move the roller skids in order to find out the rolling resistance. The maximum force on the ram was found to be less than 4 kips (17.8 kN) under a 100-kip (445 kN) vertical loading. Based on that rolling resistance, final design of the hydraulic equipment was carried out to use a smaller ram of 9-kip (40.1 kN) capacity, permitting faster loading rates.

The rolling fatigue test setup was successfully operated at static loading rates, using a servo-controlled loading system. The linearity of the long-travel linear potentiometer used for displacement control was verified. A small auxiliary control circuit connecting the potentiometer to the controller was designed, built, tested, and found to permit stable control of the roller skids.

The rolling fatigue test setup was operated at realistic dynamic loading rates of about 1 Hz for periods of time near one minute. At this loading rates, several types of mild instability became apparent which could have caused problems in prolonged fatigue testing.

To eliminate those instabilities, several kinds of successively stiffer and stronger lateral restraint were installed to prevent movement of the roller skids perpendicular to their direction of travel along the slab. Several kinds of successively stiffer lateral restraint were installed to prevent movement of the reaction frame parallel and perpendicular to the direction of travel of the roller skids along the slab.

In spite of these specific steps, the apparatus did not operate successfully at dynamic loading rates. Apparently, this is the first time that an attempt has been made to operate a full-sized, realistic, servo-controlled rolling fatigue test apparatus. In retrospect, it is possible that some of the technical difficulties associated with successful operation of such an apparatus were underestimated.

7.2 VERIFICATION OF ANALYTICAL MODEL FOR ROLLING FATIGUE TESTS

One of the important features in rolling fatigue tests was to maintain a constant axial load on the specimens regardless of the location of the roller skids. The method of doing this was described in Section 4.6, and was also verified using the analytical model discussed in Section 3.4. In this section, the predicted value is compared to the results from static rolling tests.

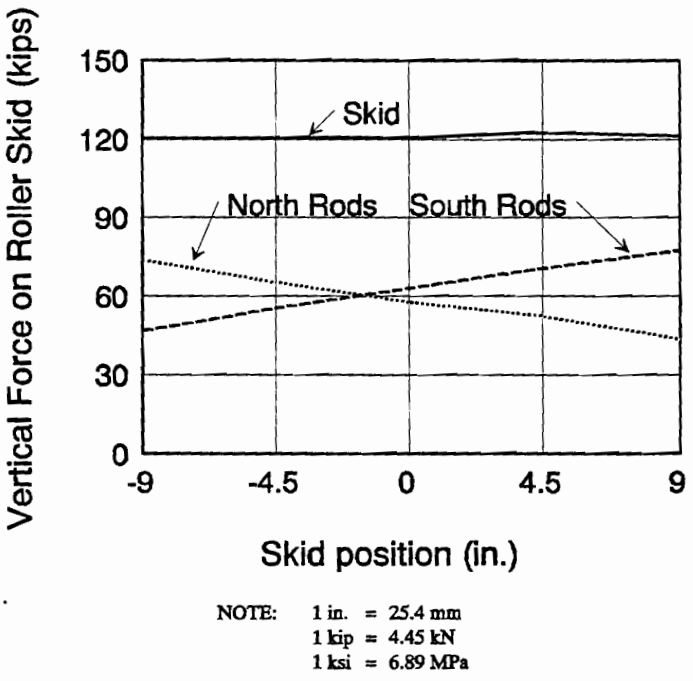

Figure 7- 1 Measured force on skids and rods, static rolling test

Readings from two strain gages installed on each tension rod were converted to the corresponding forces. The loads on the rods at each end (north and south) were then summed. The summation of measured forces on the rods at both ends was the actual compressive force imposed on the test specimen as shown in Figure 7.1. Comparison with the analytical results is shown in Figure 7.2. As shown in Figure 7.2, the measured results agree quite well with those predicted by the analytical model. While the skids moved horizontally, the load on the specimen remained constant.

7.3 CORRELATION OF PULSATING AND ROLLING FATIGUE TESTS

An important aspect of this test program was to correlate rolling and pulsating fatigue tests in terms of damage level. This was done by examining the analytical results.

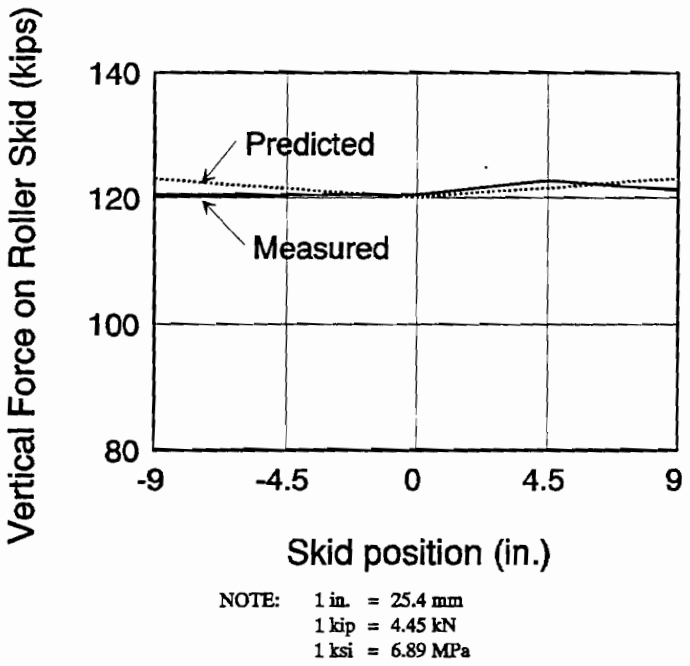

Figure 7- 2 ***Measured vs. predicted vertical force on skids, static rolling test (120-kip load)***

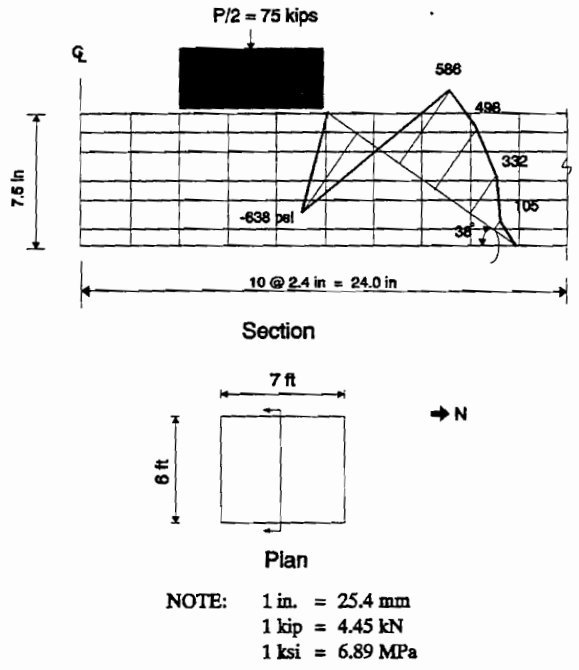

Figure 7- 3 ***Normal stresses along the assumed failure section (center of slab, east-west direction)***

Punching shear failure of bridge decks is governed by tensile stresses in concrete perpendicular to the failure section. The estimated failure section is oriented at 38 degrees to the slab surface, and extends downward from the perimeter of the loaded footprint. Normal stresses at this failure section cause punching shear failure. At a 150-kip (668 kN) load at the center of specimen, those stresses are shown in Figure 7.3. Also shown in Figures 7.4 and 7.5 are the normal stresses along the assumed failure section when a 150-kip (668 kN) load is at the middle of the specimen, and at 9 inches (229 mm) from the middle of the specimen respectively. Both figures show the normal stresses at three different locations (1.75, 3.0, and 4.25 inches (44.5, 76.2, and 108.0 mm) from the bottom of the slab), and also the average of those stresses.

Based on these analytical results, results of the rolling and pulsating tests were compared. The load range for pulsating tests was defined between a maximum load and a minimum load equal to 10 percent of the maximum. The stress range thus would be 90 percent of the stresses when the load was 150 kips (668 kN). For the rolling fatigue tests, the stresses varied as the loading point moved back and forth. For instance, the stresses at the middle of

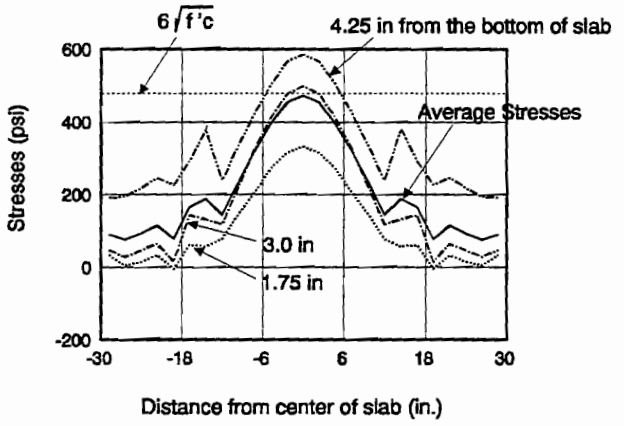

NOTE: 1 in. = 25.4 mm
1 kip = 4.45 kN
1 ksi = 6.89 MPa

Figure 7- 4 Normal stresses along the assumed failure section (P = 150 kips at center)

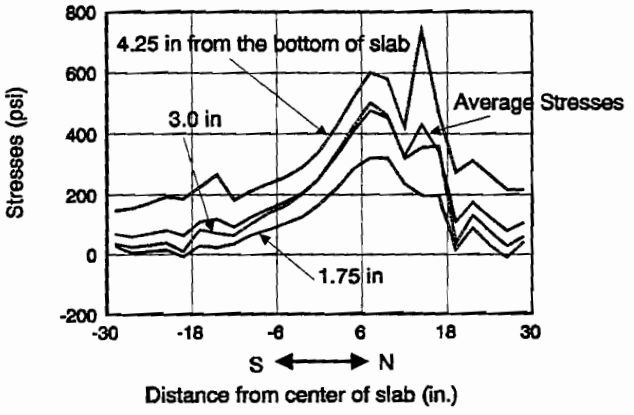

NOTE: 1 in. = 25.4 mm
1 kip = 4.45 kN
1 ksi = 6.89 MPa

Figure 7- 5 Normal stresses along the assumed failure section (P = 150 kips at 9 inches north of center)

the slab would be the highest when the load was at the center of the slab; they should be the smallest when the load was away from the center, at 9 inches (229 mm) from the center. The stress range thus would be the difference between these two limiting values.

Following this assumption, the stress range along the assumed failure section for both pulsating and rolling fatigue tests is shown in Figure 7.6. For pulsating tests, the load range is 135 kips (601 kN) (between 15 kips (67 kN) and 150 kips (668 kN)); for rolling tests, the load range comes from a 150-kip (668 kN) load moving 18 inches (457 mm). Figure 7.6 shows that the stress range for pulsating fatigue to a given maximum load is far higher than that of rolling fatigue for the same load near the middle of the slab, where the punching shear failure occurs. In other words, the pulsating test specimen will experience a higher stress range than the rolling one. Thus, higher loads must be applied to the rolling fatigue specimen in order to achieve the same stress range as in the pulsating fatigue specimen.

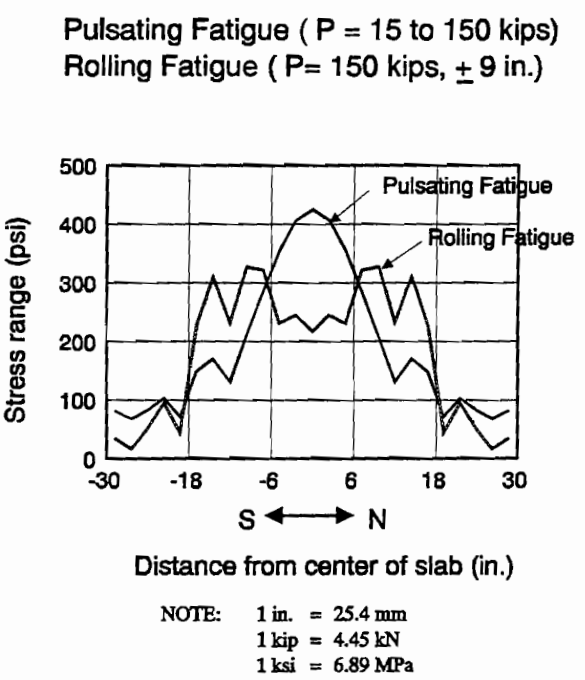

Figure 7- 6 ***Stress range along the assumed failure section for pulsating and rolling fatigue tests***

The peak stress range of the pulsating fatigue setup was 30 percent higher than that of the rolling one in Figure 7.6. This means, for instance, that pulsating fatigue tests with a 90-kip (400.5 kN) load range (between 10 kips (44.5 kN) and 100 kips (445 kN)) would have the same effect on fatigue behavior of the specimen as rolling fatigue tests with a 130-kip (579 kN) load. By comparing stress ranges produced by pulsating and rolling fatigue loads, it is possible to predict rolling fatigue behavior based on pulsating fatigue behavior.

The Japanese tests referred to in Section 2.3 were not described with sufficient details in Ref. 12 to allow analysis of their results using the finite element program described in this report. Their loading arrangement included a moving wheel load, but there was no details given to describe its distribution to the slab surface. Thus no loaded area can be assumed for determining the stresses in the slab. Furthermore, they had very different support conditions for the slabs than those used in the present study, but specific details were not given in their paper. It was stated that their slabs were restrained from corner uplift, while the slabs tested in the present study were unrestrained. There is thus no basis for making a comparison of results using the analysis described above with very limited experimental data referred in Ref. 12.

CHAPTER EIGHT

SUMMARY AND CONCLUSIONS

8.1 SUMMARY

An experimental and analytical investigation was conducted on the punching shear behavior of concrete bridge decks under static, pulsating fatigue, and rolling fatigue loads.

8.1.1 Analytical Program

Since the beginning of the program, it was considered important to develop the analytical model in order to obtain the experimental specimens which would represent the full-scale bridge decks, permitting various types of test scheme. Several analytical models were analyzed using the finite element method, based on a sequential linear approach. A model for static and pulsating fatigue tests was obtained, and the predicted results were compared with those obtained from the experimental specimen. An analytical model for the rolling fatigue setup was also studied and the results were compared with the rolling test results. These comparisons with the experimental tests showed the validity of the refined analytical models. The correlation between pulsating and rolling fatigue tests was then investigated based on the analytical results.

8.1.2 Experimental Program

The static load tests were conducted to find the ultimate capacities of the experimental specimens, which were used as zero-cycle points on the S-N curve. The specimens failed close to the predicted load level by sudden punching shear, verifying the general punching shear model based on the effect of arching action. Pulsating fatigue tests were conducted on three cast-in-place decks at a load range of 130 kips (579 kN); they failed by a punching shear as desired. The reinforcement stresses at various locations were compared to and agreed well with analytical predictions. An S-N curve was then obtained based on the static and pulsating fatigue test results. A rolling fatigue setup was developed, and preliminary tests were conducted. The results were compared to the analytical results.

8.2 CONCLUSIONS

An investigation was conducted on the punching shear behavior on fatigue for the cast-in-place reinforced concrete bridge decks and the following conclusions were drawn:

1) A refined analytical model was developed to simulate the behavior of the full-scale concrete bridge decks. The sequential linear analysis accurately predicted the

results of static tests as well as rolling fatigue tests for reinforcement stresses, showing the analytical model can be extended to other bridge deck configurations.

2) Second static test was conducted and same punching shear failure was repeated as in the first test. It showed the validity of the general punching shear model, confirming the existence of arching action in the slab.

3) Pulsating fatigue tests on three specimens were conducted and preliminary S-N curve was developed. With a series of future pulsating fatigue tests, complete S-N curve will be developed.

4) Rolling fatigue test setup was developed and implemented. Static rolling test was conducted and verified the analytical model. By comparing analytical stress ranges produced by pulsating and rolling fatigue loads, it was possible to predict rolling fatigue behavior based on pulsating fatigue behavior.

APPENDIX A

CONCRETE PROPERTIES

		Static and rolling fatigue tests	Pulsating fatigue tests
Casting date		12/23/92	7/19/93
Test date		5/17/93	3/22/94
f'_c	14 day	5360 psi (36.9 MPa)	3990 psi (27.5 MPa)
	28 day	5520 psi (38.0 MPa)	5150 psi (35.5 MPa)
	test date	5950 psi (41.0 MPa)	6200 psi (42.7 MPa)
Slump		5 in. (127 mm)	5.5 in. (140 mm)

REFERENCES

1. J. Whit, J. Kim, N. H. Burns, and R. E. Klingner, "Factors Affecting the Design Thickness of Bridge Slabs: Test Setup," Research Report CTR 1305-1, Center for Transportation Research, The University of Texas at Austin, September, 1993.

2. I.-K. Fang, J. Worley, R. E. Klingner, and N. H. Burns, "Behavior of Ontario-Type Bridge Decks on Steel Girders," Research Report CTR 350-1, Center for Transportation Research, The University of Texas at Austin, January 1986.

3. C. W. Elling, R. E. Klingner, and N. H. Burns, "Distribution of Girder Loads in a Composite Highway Bridge," Research Report CTR 350-2, Center for Transportation Research, The University of Texas at Austin, January 1986.

4. C. K.-T. Tsui, N. H. Burns, and R. E. Klingner, "Behavior of Ontario-Type Bridge Decks on Steel Girders: Negative Moment Region and Load Capacity," Research Report CTR 350-3, Center for Transportation Research, The University of Texas at Austin, January 1986.

5. K. H. Kim, R. E. Klingner, N. H. Burns, and J. Dominguez, "Behavior of Skew Bridges with Ontario-Type Decks," Research Report CTR 350-4F, Center for Transportation Research, The University of Texas at Austin, January 1988.

6. I.-K. Fang, J. Worley, R. E. Klingner, and N. H. Burns, "Behavior of Isotropic Concrete Bridge Decks on Steel Girders," Structures Journal, ASCE, vol. 116, no. 3, March 1990, pp. 659-679.

7. I.-K. Fang, C. K.-T. Tsui, N. H. Burns, and R. E. Klingner, "Fatigue Behavior of Cast-in-Place and Precast Panel Bridge Decks with Isotropic Reinforcement," PCI Journal, vol. 35, no. 3, May-June 1990, pp. 28-39.

8. R. E. Klingner, I.-K. Fang, C. K.-T. Tsui, and N. H. Burns, "Load Capacity of Isotropically Reinforced, Cast-in-Place and Precast Panel Bridge Decks," PCI Journal, vol. 35, no. 4, July-August 1990, pp. 104-114.

9. P. C. Perdikaris and S. Beim, "RC Bridge Decks under Pulsating and Moving Load," ASCE, Journal of Structural Engineering, vol. 114, no. 3, March 1988, pp. 591-607.

10. P. C. Perdikaris, S. Beim, and S. N. Bousias, "Slab Continuity Effect on Ultimate and Fatigue Strength of Reinforced Concrete Bridge Deck Models," ACI Structural Journal, vol. 86, no. 4, July-August 1989, pp 483-491.

11. Ontario Highway Bridge Design Code and Commentary, Second Edition, Ontario Ministry of Transportation and Communication, Ontario, Canada, 1983.

12. S. Matsui, et al., "Concepts for Deterioration of Highway Bridge Decks and Fatigue Studies," International Symposium on Fundamental Theory of Reinforced and Prestressed Concrete, Nanjing, China, September, 1986, pp. 831-838.

13. A. K. Azad, et al., "Loss of Punching Capacity of Bridge Deck Slabs from Crack Damage," ACI Structural Journal, vol. 90, no.1, January-February 1993, pp.37-41.

14. B. deV. Batchelor, B. E. Hewitt, and P. Csagoly, "An Investigation on Fatigue Strength of Deck Slabs of Composite Steel/Concrete Bridges," Transportation Research Record, no. 664, 1978, pp.153-161.

15. J. S. Kuang and C. T. Morley, "Punching Shear Behavior of Restrained Reinforced Concrete Slabs," ACI Structural Journal, vol. 89, no. 1, January-February 1992, pp.13-19.

16. E. Wilson, and A. Habibullah, "SAP90^{TM} -- A Series of Computer Programs for the Static and Dynamic Finite Element Analysis of Structures," Computers and Structures, Inc., Berkeley, California, 1990.

17. P. R. Johnston, and W. Weaver, Finite Elements for Structural Analysis, Prentice Hall, 1984.

18. Standard Specifications for Highway Bridges, 13th Edition, American Association of State Highway and Transportation Officials, 1983.

19. Building Code Requirements for Reinforced Concrete and Commentary, American Concrete Institute, ACI 318-89 and ACI 318R-89.

20. Standard Specifications for Construction of Highways, Streets, and Bridges, Texas Highway Department, 1972.

21. G. P. Mallet, Fatigue of Reinforced Concrete, HMSO, London, 1991.

22. H. Kupfer, H. K. Hilsdorf, and H. Rusch, "Behavior of Concrete under Biaxial Stresses," ACI Journal, vol. 66, August 1969, pp.656-666.

23. J. W. Murdock, "A Critical Review of Research on Fatigue of Plain Concrete," Engineering Experiment Station Bulletin No. 475, University of Illinois, Urbana, Illinois, 1965.

24. J. P. Lloyd, J. L. Lott, and C. E. Kesler, "Fatigue of Concrete," Engineering Experiment Station Bulletin No. 499, University of Illinois, Urbana, Illinois, 1968